ELSEVIER

Earth and Planetary Science Letters 204 (2002) 183–202

EPSL

www.elsevier.com/locate/epsl

Modeling the distribution of isotopic ratios in geochemical reservoirs

James B. Kellogg *, Stein B. Jacobsen, Richard J. O'Connell

Department of Earth and Planetary Sciences, Harvard University, 20 Oxford Street, Cambridge, MA 02138, USA

Received 19 December 2001; accepted 5 August 2002

Abstract

We present an extension of the conventional geochemical reservoir model for the evolution of the Earth's crust–mantle system in which we calculate not only the mean isotopic ratios, but also the distribution of those ratios within the reservoirs. Owing to low chemical diffusion rates, subreservoirs that are created by mass transport into and out of the mantle effectively exist as distinct geochemical entities for all time. By tracking these subreservoirs, we obtain a model of the full range of isotopic values represented in the mantle. Using results from numerical calculations of mixing, we also track the length scales associated with each subreservoir. Applying simple statistics, we obtain the distribution of expected measurements as a function of the stirring time, effective melt fraction, sampling volume, and mass transport history. We present calculations of isotopic heterogeneity for two simple mantle evolution models and explore the sensitivity of geochemical observables to the variables mentioned. We focus on the Rb–Sr and Sm–Nd systems and are able to reproduce much of the observed complexity of oceanic basalts. We infer that the stirring time of the mantle falls between 250 and 750 Myr, and that the initial length scale of mantle heterogeneity before stirring is of the same order as the length scale of sampling. We also conclude that the differences between isotopic data from mid-ocean ridge basalts and ocean island basalts cannot simply be due to differences in sampling volume, but must also reflect differences in the source reservoirs and/or melting processes. Increasing the size of the ocean island basalt source region by 45% with respect to the mid-ocean ridge basalt source region reproduces the offset between the two distributions, but still fails to explain the more isotopically extreme measurements. Our results show that the argument suggesting that the absence of samples with a primitive isotopic signature indicates that no primitive material remains in the mantle is not valid.

Keywords: mixing; heterogeneity; strontium; neodymium; models; mantle; isotope ratios

1. Introduction

The apparently contradictory evidence of geophysics and geochemistry has long complicated efforts to understand the evolution of the Earth's mantle (for recent reviews, see [1–3]). For example, the standard layered geochemical model of the mantle appears to be inconsistent with high-reso-

* Corresponding author. Tel.: +1-617-495-8986; Fax: +1-617-495-8839.
E-mail address: kellogg@geophysics.harvard.edu (J.B. Kellogg).

0012-821X/02/$ – see front matter
PII: S0012-821X(02)00981-0

lution seismic tomography and other geophysical data that indicate whole-mantle flow. However, with the whole-mantle convection model favored by most geophysicists, it is difficult to satisfy the constraints of geochemistry, particularly the isotopic mass balance of the rare earth elements and the noble gases. Resolving this issue requires simultaneous improvement of both the data sets and the models used to understand them.

We focus here on the measurements of Nd and Sr isotopic ratios in oceanic basalts, as shown in Fig. 1. Efforts to understand this array of data have generally focused on two features: the roughly linear relationship between the Nd and Sr isotopic systems [5–7], and the end members of the distribution (e.g. [4]). We believe there is more information contained in these data, but we need to develop quantitative models to extract it.

An important modeling tool used by geochemists for some time has been geochemical reservoir modeling [8–15]. To a first approximation the Earth may be broken into a number of homogeneous reservoirs with mass transported between them, subject to chemical fractionation effects. This parameterization allows one to track the average chemical/isotopic evolution of the various reservoirs through time and constrain this evolution using observational chemical/isotopic data from both young and old rocks.

While popular among geochemists, this technique has been slow to gain favor among geophysicists. A significant amount of geophysical modeling has focused on the behavior of tracers within a full convective system. The tracers range from passive particles [16–18], to strain markers [19–21], to passive tracers carrying chemical/isotopic information [22,23], to chemical/isotopic tracers which also affect the density field [24–26]. This last category, thermochemical convection, is computationally expensive and technically challenging (e.g. [27]), but has yielded significant insight, particularly into the dynamics of a hypothetical deep layer in the mantle.

Allègre and Lewin [28] and Allègre et al. [29] attempted to use the variance in the isotopic data by relating it to the stirring time (analogous to the mixing time scale of [30]). They did this by essentially creating reservoir models for heterogeneity; within each reservoir there were source and sink terms for chemical variance. These source terms depended on the mass transport between the reservoirs. However, they were considered unknown and canceled out of the problem. Furthermore, the models included the effect of sampling length scale only indirectly (it is bound up in Olson et al.'s mixing time scale), obscuring its importance to the problem.

In this work, we use the conventional reservoir formulation to model the evolution of the bulk geochemical reservoirs. We then investigate the heterogeneity created within the Earth's mantle by mass transport between the bulk reservoirs. This extension is, by design, limited. We allow the bulk evolution to control the growth of heterogeneity, but we do not allow the heterogeneities to affect the bulk evolution. We then address the question of how the heterogeneous mantle will appear when sampled on a finite length scale by present-day melting. Ultimately, we generate synthetic geochemical data which we compare directly with the real data shown in Fig. 1.

2. Methods and application to the case of uniform crustal growth

In this section, we derive our extended reservoir model and apply it to one of the simplest scenarios for Earth evolution: a linear extraction of the continental crust from a limited region of the mantle with no crustal recycling (Model II of [8].) In this scenario, only roughly 1/3 of the mantle is depleted, whereas the rest of the mantle remains primitive. This depleted mantle fraction is at the low end of current estimates based on mass balance constraints [31] and may not be easily reconcilable with modern seismic tomography. However, we want to stay as close to previous modeling efforts as possible while building this model.

2.1. Conventional box models

Our method for the modeling of average reservoir evolution follows that laid out previously [8,11].

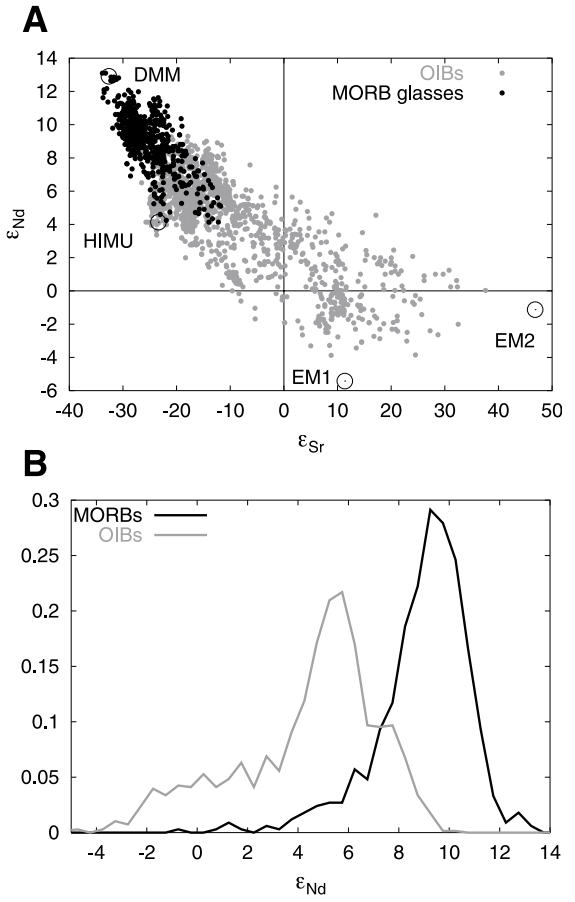

Fig. 1. (A) Measurements of Nd and Sr isotopes in mid-ocean ridge basalt (MORB) glasses and ocean island basalts (OIBs) from the PetDB and GeoROC databases. MORB data are partially obscured by the OIB data. Large circles show the isotopic compositions of proposed mantle components (e.g. [4]). The classical anti-correlation between ε_{Nd} and ε_{Sr} is evident, as are higher-order features, such as a general concavity and increased heterogeneity away from the DMM end member. (B) Normalized histograms of the real data, binned at 0.5 ε units. The MORB curve is close to Gaussian, although skewed slightly left. The OIB curve has a significantly lower mode and is much more skewed left (although the non-random sampling on which this curve is based makes interpretation difficult). Note that there are essentially no measurements of ε_{Nd} in the OIBs that plot to the right of the mode of the MORB curve.

For each isotopic system (e.g. Sm–Nd, Rb–Sr) we identify three types of species, denoted *r*, *d*, and *s*. These represent the radioactive parent isotope, the stable, radiogenic daughter isotope, and the stable, non-radiogenic isotope, respectively. We divide the Earth into a small number of major reservoirs numbered 1–4, representing the Bulk Silicate Earth (BSE), depleted mantle, continental crust, and undepleted or enriched mantle as shown in Fig. 2. We avoid the terms 'upper' and 'lower' mantle, because geochemical reservoir models do not by themselves constrain the geometries of the reservoirs, only their masses and the transport between them.

We define N_{ij} to be the number of atoms of species i residing in reservoir j. We combine the N_{ij}s to obtain the following three quantities:

$$\varepsilon = \left(\frac{N_{dj}/N_{sj}}{N_{d1}/N_{s1}} - 1\right) \times 10^4 \tag{1}$$

$$f_j^{r/s} = \frac{N_{rj}/N_{sj}}{N_{r1}/N_{s1}} - 1 \tag{2}$$

$$E_{sj} = \frac{C_{sj}}{C_{s1}} \tag{3}$$

The mass of reservoir j is M_j, and the mass transport from reservoir i to reservoir j is $\dot{M}_{ij}$. The concentration of species i in reservoir j is:

$$C_{ij} = \frac{N_{ij}}{M_j} \tag{4}$$

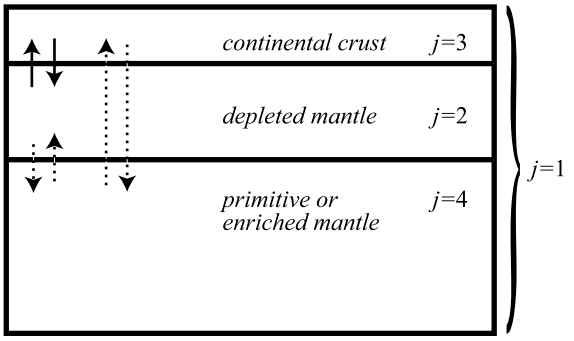

Fig. 2. Cartoon of the conventional reservoir model geometry with a homogeneous crust and depleted upper mantle overlying a primitive or enriched lower mantle. In the general case, there is bidirectional mass transport between each pair of reservoirs. In the models presented here, however, Reservoir 4 will remain completely isolated. This cartoon is conceptual only; reservoir models may be used to determine the volume of the reservoirs and the mass transport between them, but may not constrain the geometry.

Partial melting creates different chemical concentrations in the liquid and solid. To account for this difference, we define c_{ik} as the concentration of species i in a new parcel of mass added to reservoir k from reservoir j and also:

$$d_{ijk} = \frac{c_{ik}}{C_{ij}} \tag{5}$$

which represents the enrichment of species i in the transported parcel relative to the source reservoir. We assume that mass fractionation effects are negligible, so $d_{sjk} = d_{djk}$ (i.e. there is no fractionation between isotopes of the same element). In single stage melting, d_{ijk} is related simply to the degree of partial melting F and the bulk partition coefficient, D_i. Here we treat it as a free parameter that can be adjusted so that a given transport history yields the observed present-day isotopic compositions of the various reservoirs.

The time evolution of the reservoirs is controlled by the following coupled ordinary differential equations (ODEs):

$$\frac{\mathrm{d}M_j(t)}{\mathrm{d}t} = \sum_{k=1}^{n_{\mathrm{res}}} [\dot{M}_{kj}(t) - \dot{M}_{jk}(t)] \tag{6}$$

$$\frac{\mathrm{d}N_{sj}(t)}{\mathrm{d}t} = \sum_{k=1}^{n_{\mathrm{res}}} [\dot{M}_{kj}(t) d_{skj} C_{sk}(t) - \dot{M}_{jk}(t) d_{sjk} C_{sj}(t)] \tag{7}$$

$$\frac{\mathrm{d}N_{rj}(t)}{\mathrm{d}t} = \sum_{k=1}^{n_{\mathrm{res}}} [\dot{M}_{kj}(t) d_{rkj} C_{rk}(t) - \dot{M}_{jk}(t) d_{rjk} C_{rj}(t)] - \lambda_r N_{rj}(t) \tag{8}$$

$$\frac{\mathrm{d}N_{dj}(t)}{\mathrm{d}t} = \sum_{k=1}^{n_{\mathrm{res}}} [\dot{M}_{kj}(t) d_{skj} C_{dk}(t) - \dot{M}_{jk}(t) d_{sjk} C_{dj}(t)] + \lambda_r N_{rj}(t) \tag{9}$$

where λ_r is the decay constant for the radioactive isotope r, and n_{res} is the number of reservoirs, taken to be 4 in this paper, as shown in Fig. 2. If we do this for n_{sys} isotopic systems, we get a total of $n_{\mathrm{res}}+3n_{\mathrm{sys}}n_{\mathrm{res}}$ coupled ODEs that we solve simultaneously using a fifth-order Runge–Kutta scheme (e.g. [32]) starting from an initially undifferentiated (chondritic) Earth.

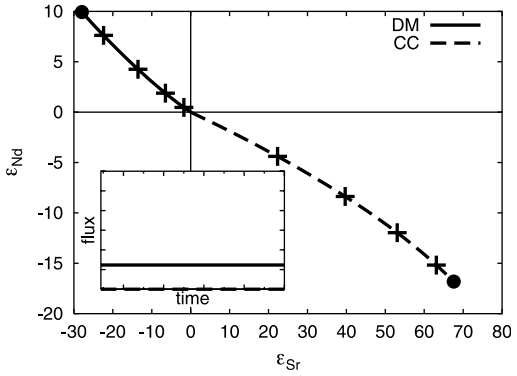

Fig. 3. Evolution of ε_{Nd} and ε_{Sr} in the mean depleted mantle (DM) and continental crust (CC). Crosses are placed at 1 Gyr intervals, and circles represent the present-day composition of the average DM and CC. The rather uninteresting inset figure shows the assumed mass transport history: the solid curve shows the rate of mass transport from the depleted mantle to the continental crust (here constant), while the dashed line (here identically zero) shows the rate of crustal recycling. The transport history corresponds to Model II of [8].

Jacobsen and Wasserburg [8] proposed a simple reference model of unidirectional mass transport in which the continental crust is extracted from a limited region of the mantle (representing roughly 1/3 of the bulk silicate Earth (BSE)). The temporal evolution of this model in ε_{Nd}–ε_{Sr} space is shown in Fig. 3. The parameters for this and all other calculations are listed in Table 1.

2.2. Creating heterogeneity in the mantle

Mantle chemical heterogeneity can be created in two ways (illustrated in Fig. 4): partial melting within the mantle and the influx of material from outside the mantle. Partial melting events yield two distinct components: a melt and a residue. For simplicity, we only consider the melting associated with the creation of continental crust. In this case, melt is transported out of the mantle and added to the mean continental crust. The residue, however, stays behind.

There is still debate as to the actual mechanism by which continental crustal growth occurs, and the process may well have changed since the Archean (for a recent review, see [33]). Given the complexity and the lack of consensus on the mechanism, we will adopt a very simple model of crustal growth: a simple one-stage, small-degree melt, leaving behind a single uniform residue. While this simplification does not closely approximate processes such as intracrustal differentiation and subsequent delamination, it should capture the first-order behavior of systems dominated by subduction zone processes, assuming the residual material enters the mantle as a roughly coherent, if heterogeneous, package.

In all models presented here, we consider roughly 2/3 of the mantle to be isolated throughout Earth history. Therefore, the only material injected into the depleted mantle originates in the continental crust. While the crust is observably heterogeneous itself, we will treat it as a uniform reservoir. In the Earth, chemical differences within the recycled crustal component are likely small compared with the difference between the bulk continental crust and depleted mantle.

Once created, these chemical heterogeneities represent 'subreservoirs' within the main depleted mantle reservoir. They will not diffuse into the rest of the mantle on a scale greater than 1 km [34,35], and therefore they each evolve chemically as a closed system.

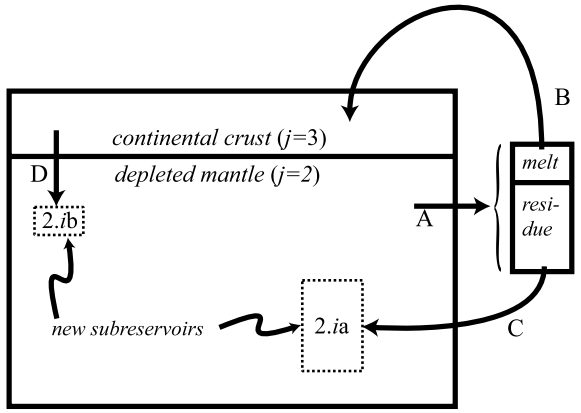

Fig. 4. Cartoon illustrating our model for the creation of subreservoirs in the depleted mantle. (A) At each time step, we partially melt a portion of the bulk depleted mantle (Reservoir 2) to create a chemically fractionated melt and residue. (B) The melt is added to the mean crust (Reservoir 3), whereas (C) the residue is put back into the depleted mantle, resulting in the creation of a new subreservoir (2.*i*a). (D) In addition, continental crust may be recycled into the depleted mantle, creating another subreservoir (2.*i*b).

Table 1
Present-day values of parameters used in the calculations

Parameter	Sm–Nd	Rb–Sr	Sys. independent	See Eq. #
M_2/M_1			0.3050	4
M_3/M_1			0.0056	4
τ_{stir}			500 Myr[a]	26
l^o_{h23}			100 km	26
l^o_{h32}			10 km	26
λ_r	0.00654 Ga^{-1}	0.0142 Ga^{-1}		8
N_{r1}/N_{s1}	0.1967	0.0827		1
N_{d1}/N_{s1}	0.511847	0.7045		1
C_{s1}	1.26 ppm	22 ppm		4
d_{ijk}	1[b]	1[b]		5
Linear evolution, with no recycling of continental crust (CC)				
d_{r23}	16.5	72.0		
d_{s23}	25.5	19.1		
Time-dependent evolution, with recycling of mean CC				
d_{r23}	14.2	200.0		
d_{s23}	28.3	21.5		
Time-dependent evolution, with recycling of fractionated CC				
d_{r23}	6.0	200.0		
d_{s23}	28.8	15.1		
d_{r32}	1.7	2.0		
d_{s32}	1.7	0.7		

Equation references in rightmost column indicate the first appearance of the parameter; definitions can be found there. Masses and elemental concentrations taken from [11].
[a] Unless otherwise noted in text.
[b] Except parameters listed in this table.

2.2.1. Derivation of the model

To calculate the evolution of mantle heterogeneity, we use a discrete time history with steps $\Delta t = 100$ Myr. At each time step, we calculate the mean isotopic composition of the continental crust and depleted mantle as described above, and also quantify the mass and composition of any new subreservoirs created. We consider all the residue created during this time step to constitute a single uniform subreservoir and do likewise for all crust recycled during this time step.

Quantitatively, the mass of the residual subreservoir created at t_i is:

$$m_{2.i\mathrm{a}} = (F^{-1}-1)\dot{M}_{23}\Delta t \tag{10}$$

where F is the effective degree of partial melting. Estimates of the degree of partial melting in mid-ocean ridge environments and subduction zones are on the order of 0.1. However, our effective F likely reflects the net result of two or more melting events and therefore will likely be significantly less than this value. For example, two melting events of 0.1 apiece will yield an effective F of $\sim 0.1\times 0.1 = 0.01$. In addition, the enrichment of incompatible elements in the continental crust places strict upper bounds on this number; we discuss this more fully in Section 3.1.

The isotopic composition of the subreservoir is:

$$\varepsilon_{d2.i\mathrm{a}} = \varepsilon_{d2} \tag{11}$$

$$f^{r/s}_{2.i\mathrm{a}} = \frac{1-Fd_{r23}}{1-Fd_{s23}}(f^{r/s}_{2}+1)-1 \tag{12}$$

$$E_{2.i\mathrm{a}} = \frac{1-Fd_{s23}}{1-F}E_2 \tag{13}$$

From these equations, we can see that in the absence of chemical fractionation (i.e. $d_{ijk} = 1$), the melting process will not create heterogeneity in the depleted reservoir. Chemical fractionation is key to the development of isotopically distinct subreservoirs.

The mass of the subreservoir created by the recycling of continental crust at t_i is:

$$m_{2.i\mathrm{b}} = \dot{M}_{32}\Delta t \tag{14}$$

Its isotopic composition is:

$$\varepsilon_{d2.i\mathrm{b}} = \varepsilon_{d3} \tag{15}$$

$$f^{r/s}_{2.i\mathrm{b}} = \frac{d_{r32}}{d_{s32}}f^{r/s}_{3} \tag{16}$$

$$E_{2.i\mathrm{b}} = d_{s32}E_3 \tag{17}$$

Note that the composition reflects that of the mean continental crust; we do not calculate the heterogeneity within the continental crustal reservoir. Also, chemical fractionation plays only a secondary role in the creation of heterogeneity through crustal recycling. Even if the recycled material undergoes no chemical fractionation, it will represent a source of heterogeneity, assuming that the isotopic composition of the continental crust is distinct from that of the depleted mantle.

Initially, Reservoir 2 is composed entirely of primitive material. Mass balance requires that the mass of primitive material in Reservoir 2, m_2^{prim}, as a function of time obeys:

$$m_2^{\mathrm{prim}} = M_2 - \sum_i m_{2.i} \tag{18}$$

where we have dropped the subscripts a and b because the distinction between them is no longer necessary.

Because each of the subreservoirs represents a closed system, $f^{r/s}_{2.i}$ and $E_{2.i}$ remain constant with time, whereas $\varepsilon_{d2.i}$ evolves through radioactive decay according to:

$$\frac{\mathrm{d}\varepsilon_{d2.i}}{\mathrm{d}t} = (f^{r/s}_{2.i}-\varepsilon_{d2.i}\times 10^{-4})Q^{*}_{d} \tag{19}$$

which has the solution:

$$\varepsilon_{d2.i}(t) = \varepsilon_{d2.i}(t^{o}_{2.i} + \frac{Q^{*}_{d}(t)}{\lambda_r}f^{r/s}_{2.i}\,(\mathrm{e}^{\lambda_r(t-t^{o}_{2.i})}-1) \tag{20}$$

where

$$Q^{*}_{d}(t) = \frac{N_{r1}(t)}{N_{d1}(t)}\lambda_r\times 10^4 \tag{21}$$

is a bulk Earth parameter, and $t^{o}_{2.i}$ is the time of the subreservoir's creation.

Physically, the subreservoirs are simply part of the general mantle flow. Therefore, when the depleted mantle is melted to generate new continental crust, portions of the subreservoirs may be partially melted. On average, each subreservoir will contribute to the melt region in proportion to its mass and the mass of the melt region. The mass of the melt region at time t_i is:

$$m_{\mathrm{melt}} + m_{\mathrm{residue}} = \dot{M}_{23}F^{-1}\Delta t \tag{22}$$

Therefore, the mass of each subreservoir evolves according to:

$$\frac{dm_{2.i}}{dt} = -\frac{m_{2.i}}{M_2}\dot{M}_{23}F^{-1} \quad (23)$$

This description is entirely consistent with the conventional reservoir model formulation in which additions to the continental crust represent fractionated material from the average depleted mantle. This agreement leads to a new interpretation of the conventional reservoir models: they do not require that the reservoirs be perfectly (or even well) mixed. Rather, they require that there be no bias in the sampling of the various regions within the reservoirs, each region has an equal chance of being included in a mass-transfer event so that on average the material being exchanged represents the mean composition of the source reservoir.

This assumption of a bias-free mantle could break down in two respects. First, more fertile material is more likely to contribute to the melt portion of a melt–residue pair than previously melted, depleted material. This complexity has been ignored in all previous reservoir-modeling efforts of which we are aware, and we will continue to neglect it here, although it may be an important effect to include in future work. Second, it may be reasonable to expect a time-lag between the depletion and likely re-sampling of a subreservoir associated with the transit of the subresevoir through the mantle before being re-melted near the surface. However, given that our time steps are of the order of the transit time of the mantle for whole-mantle flow ($\sim$100 Myr) and also that patterns of return flow in the mantle are very complex [36], we believe that errors introduced by the neglect of this effect are minimal.

2.2.2. *Application to the simple transport history*

Applying this methodology to the simple case of linear crustal extraction, we obtain an array of isotopic compositions, as shown in Fig. 5A. The light gray curve in this figure shows the evolution of the mean depleted mantle through time (this is identical to the curve in Fig. 3. The dark curves

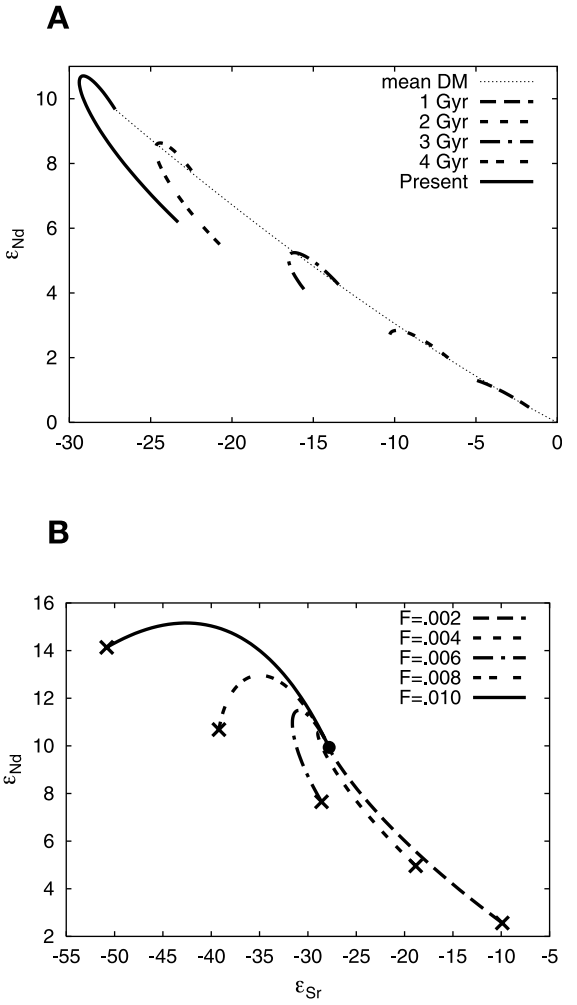

Fig. 5. The spectrum of heterogeneity generated in the depleted mantle by linear crustal extraction with no recycling. (A) The light gray curve shows the evolution of the mean isotopic values as in Fig. 3. The dark curves show full range of subreservoir isotopic values at (from right to left) 1 Gyr, 2 Gyr, 3 Gyr, 4 Gyr, and present day, assuming the melt fraction F is 0.005. Continuous curves are drawn through discrete points which represent the isotopic composition of the individual subreservoirs. (B) Curves here show present-day heterogeneity in the depleted mantle given melt fractions of (from right to left) 0.002, 0.004, 0.006, 0.008, and 0.010. (The solid curve in A would fall between the $F=0.004$ and $F=0.006$ curves.) The cross at the end of each curve represents the isotopic composition of the oldest subreservoir, whereas the circle at the intersection of the curves shows the isotopic composition of the most recently formed subreservoir (and the composition of the mean DM). Note that the relationship between age and isotopic composition is highly non-linear and that results are highly dependent on F.

are drawn through the isotopic composition of all the subreservoirs present in the depleted mantle at different stages in the system's history. For example, the solid curve is drawn through all the subreservoirs in the system at the present day. In addition, the depleted mantle will contain some volume of primitive material, in accordance with Eq. 18.

It is striking that the curves are so non-linear; there is not a simple relationship between the age of a subreservoir and its isotopic composition. This is due to the fact that the source from which the subreservoirs are derived is being continuously depleted; melt is not simply extracted from primitive material (as was done in Model I of [8]).

The tips of all five dark curves (the ends farthest from the mean evolution curve) correspond to the same subreservoir evolving through time, specifically the first one created. It is worth noting that these points all lie very close to a straight line. This is a consequence of Eq. 20, which, to first order in $\lambda_r t$, yields:

$$\varepsilon_{d2.i}(t) = \varepsilon_{d2.i}(t^o_{2.i}) + Q^*_d(t) f^{r/s}_{2.i}(t - t^o_{2.i}) \tag{24}$$

so that

$$\varepsilon_{\mathrm{Nd}2.i}(t) = [\varepsilon_{\mathrm{Sr}2.i}(t) - \varepsilon_{\mathrm{Sr}2.i}(t^o_{2.i})] \frac{Q^*_{\mathrm{Nd}}(t) f^{\mathrm{Sm/Nd}}_{2.i}}{Q^*_{\mathrm{Sr}}(t) f^{\mathrm{Rb/Sr}}_{2.i}} + \varepsilon_{\mathrm{Nd}2.i}(t^o_{2.i}). \tag{25}$$

Because $f^{\mathrm{Sm/Nd}}_{2.i}$ and $f^{\mathrm{Rb/Sr}}_{2.i}$ are of opposite sign, the slope of the straight line so described is negative.

Fig. 5B illustrates the effect of changing the melt fraction F. Each curve corresponds to the spectrum of isotopic heterogeneity expected in the depleted mantle at the present day for a given value of F, ranging from 0.002 to 0.010. If F is large, the volume of mantle which is needed to produce a given volume of melt is small, and the depletion in the residue is large. The high degree of depletion in the large-F case is evident in the extreme isotopic character of the oldest subreservoirs in Fig. 5B.

Marked in Fig. 5B with a cross is the oldest subreservoir present in each system. It is important to note that this subreservoir does not necessarily represent the most isotopically extreme component of the mantle. This is an interesting point which, to our knowledge, has not been previously noted. For example, the dashed curve representing $F = 0.002$ shows the oldest subreservoir plotting almost on a straight line between the mean depleted mantle and primitive mantle.

Because our melting model is a simplification of a complex, multi-stage, and possibly time-dependent process, it is difficult to argue strongly for a specific value of F. Instead, we show results from a range of values and identify this as an area for improvement in future generations of this model.

2.3. Mixing and sampling of subreservoirs

The curves in Fig. 5 represent the observations we would expect if we were to sample our model mantle on a point scale. The basalts we observe on the Earth surface, however, are the end result of a melting process which samples the mantle over a finite scale, thereby mixing any number of components. If we are to compare our model results with observations, we need to model this sampling process. This requires understanding the spatial evolution of the subreservoirs.

2.3.1. The parameterization of mixing

For simplicity, we consider an initially spherical subreservoir of radius $l_{\mathrm{h}2.i}$ deforming in the mantle flow, as shown schematically in Fig. 6A. (Note that this assumption of sphericity is merely for illustration; a blob of virtually any starting shape will behave in roughly the same way.) With time, the subreservoir will become stretched, thinned, and folded, ultimately leading to a 'marble-cake' structure as discussed by [37]. There are two length scales evident at each stage in Fig. 6A. The long axis, in most cases, will be significantly longer than any length scale of interest (i.e. the sampling length scale), and therefore may be neglected. The short axis, on the other hand, is central to the sampling problem.

Studies of mixing in the mantle have often focused on the question of whether stretching is in the turbulent or laminar regime (e.g. [30,38]). In the former case, the evolution of the short length

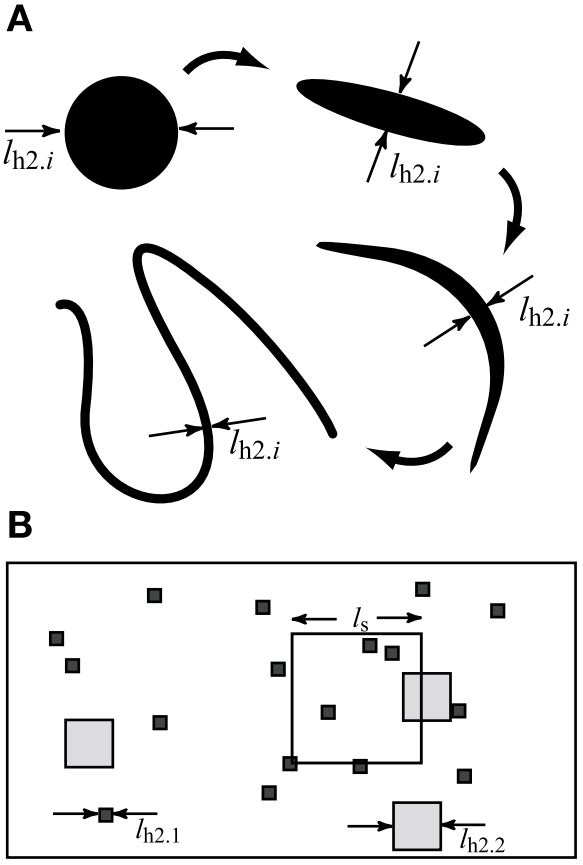

Fig. 6. Two-dimensional cartoons illustrating the mixing and sampling models. (A) Time evolution (clockwise from top left) of a single subreservoir as it is distorted in the mantle flow. The long axis of the distorted ellipse is, in general, longer than any sampling length scale of interest and can be ignored. The length of the short axis, $l_{h2.i}$, decreases exponentially with a characteristic time constant τ_{stir}. (B) Illustration of sampling in a reservoir containing two isotopically and chemically distinct subreservoirs of comparable total mass but different length scale. We break each subreservoir into a number of sub-subreservoirs of volume $l^3_{h2.i}$ which we assume to be scattered randomly throughout the mantle. We then ask the following statistical questions: how many sub-subreservoirs of each variety are contained in a box of volume l^3_s placed randomly in the reservoir, and what is the resultant chemical/isotopic composition of the box? We repeat this process for an arbitrary number of samples.

scale of a subreservoir, $l_{h2.i}$, would behave as:

$$l_{h2.i} = l^o_{hjk} e^{(-t-t^o_{2.i})/\tau_{stir}} \quad (26)$$

where l^o_{hjk} is the initial length scale of the heterogeneity, $t^o_{2.i}$ is the time at which the subreservoir was created, and τ_{stir} is the characteristic time scale of stirring. This is the time required for the short length scale to decrease by a factor of e.

In the laminar case, $l_{h2.i}$ would evolve according to:

$$l_{h2.i} = l^o_{hjk} \frac{1}{\sqrt{1 + [\dot{\varepsilon}(t-t^o_{2.i})]^2}} \quad (27)$$

where $\dot{\varepsilon}$ is the average strain rate of the system. In general, mixing in the laminar regime is much slower than that in the turbulent regime.

In three dimensions, the inclusion of toroidal motion enhances mixing and places mixing in the turbulent regime even for steady state flows [39], although isolated regions of laminar mixing may persist [36,40]. Accordingly, we will use Eq. 26 in calculating the length scales. As a nominal value for τ_{stir} we will use 500 Myr, in accordance with numerical experiment [41], but we vary this value and investigate the system's sensitivity to this parameter in Section 3.3.

2.3.2. The sampling function

Having parameterized the spatial character of the subreservoirs, we can approach the sampling problem. We ask the following question: if we place a sampling box of volume l_s randomly in the mantle (simulating a melting event at the surface), what is its composition?

We proceed by breaking each subreservoir into a number $n_{2.i}$ of sub-subreservoirs, each of volume $l^3_{h2.i}$ such that:

$$n_{2.i} = \frac{m_{2.i}}{\rho l^3_{h2.i}} \quad (28)$$

where ρ is the density. We then assume that these sub-subreservoirs are scattered randomly throughout the mantle (we have no information as to where in the reservoir each sub-subreservoir resides). Conceptually, we move the sampling volume around the mantle and determine the contribution of each subreservoir to its mass, as illustrated in Fig. 6B. In practice, we reduce the problem to one of geometrical statistics.

First, we randomly select one subreservoir on

which to focus and determine whether $ls > l_{h2.i}$ or vice versa. If the former case holds, then each sub-subreservoir could lie completely within, partially overlap, or be completely outside the sampling volume. The probability of each option is, respectively:

$$p_{in} = \frac{(l_s - l_{h2.i})^3}{V_{tot}} \tag{29}$$

$$p_{edge} = \frac{(l_s + l_{h2.i})^3}{V_{tot}} - p_{in} \tag{30}$$

$$p_{out} = 1 - p_{in} - p_{edge} \tag{31}$$

where V_{tot} is the total volume of the depleted reservoir.

Assuming that $m_{2.i} \ll M_2$ and $l^3_{h2.i} \ll l^3_s$, we can treat the location of each sub-subreservoir as an independent event (in practice, this is not a strict condition; we find that this method works for all $l_{h2.i} \leq l_s$). To find the number of sub-subreservoirs lying completely within the sampling volume, we effectively conduct $n_{2.i}$ trials of an experiment with probability p_{in} of success. This situation yields the binomial distribution, whereby the probability of q successes is:

$$p(q) = \binom{n_{2.i}}{q} p^q_{in} (1 - p_{in})^{n_{2.i} - q} \tag{32}$$

We pick a random number from such a distribution (a binomial deviate) to determine the number of sub-subreservoirs contained within the sampling volume.

In the case of large $n_{2.i}$ and small p_{in} we can approximate the binomial with the Poisson distribution, according to which the probability of q successes is:

$$p(q) = \frac{e^{\mu}\ \mu^q}{q!} \tag{33}$$

where

$$\mu = n_{2.i} p_{in} \tag{34}$$

$$= \frac{m_{2.i}}{M_2} \left(\frac{l_s}{l^o_{hjk}} e^{(t - t^o_{2.i})/\tau_{stir}} - 1 \right)^3 \tag{35}$$

is the mean number of successes.

The case in which the sub-subreservoirs only partially overlap the sampling volume is slightly more complicated in that we must calculate the degree of overlap for each sub-subreservoir (or a statistical description thereof). The details of this part of the calculation are not central to the present discussion.

After calculating the total volume that a given subreservoir contributes to the sampling volume, $v^{samp}_{2.i}$, we adjust the sampling length scale and the total reservoir volume as:

$$l'_s = (l^3_s - v^{samp}_{2.i})^{1/3} \tag{36}$$

$$V'_{tot} = V_{tot} - v^{samp}_{2.i} \tag{37}$$

where the unprimed variables represent the old values and the primed variables represent the new. This adjustment takes care of the fact that the sampling of different subreservoirs are not truly independent events.

All of the above can be easily generalized for the case in which $l_{h2.i} > l_s$.

This procedure is repeated for all subreservoirs, or until the sampling volume is completely full. In the latter case, we move immediately to calculating the isotopic composition of the sample. In the former case, we first fill the remaining sample volume with primitive material and then calculate the chemical characteristics.

By running the sampling algorithm numerous times, we are able to generate an array of synthetic geochemical data, predicting the distribution of results one would expect from measuring samples of the depleted mantle given a set of starting assumptions. This ability to create synthetic data greatly facilitates the comparison of model results with real data, allowing a fuller evaluation of the model.

It is instructive at this stage to investigate the non-dimensional parameters that control the sampling. Eq. 33 shows that, to the extent that the

Poisson approximation to the binomial distribution is valid, these parameters are three: $m_{2.i}/M_2$, $\tau_{\mathrm{stir}}/(t-t^{\mathrm{o}}_{2.i})$, and $l_{\mathrm{s}}/l^{\mathrm{o}}_{\mathrm{h}jk}$. The first two are different for each subreservoir and depend on the details of the flux history. In principle, these could be related to the mean age of the subreservoirs in general, but it is not clear that such a relation makes the parameterization any more transparent. The third parameter, $l_{\mathrm{s}}/l^{\mathrm{o}}_{\mathrm{h}jk}$, is more useful; it appears that we need not specify absolute length scales for l_{s} and l_{h}, but rather just the ratio between them. However, this simplification breaks down along with the Poisson approximation if $n_{2.i}$ is small. In that case, Eqs. 28, 29 and 32 show that the ratio $\rho(l^{o}_{\mathrm{h}jk})^3/m_{2.i}$ is also relevant. Because of this complexity, we will show results with particular values of l_{s} and l_{h}. Specifically, we assume that the l^{o}_{h} is 100 km for residual mantle and 1/10 that for recycled mantle. If one translates the results shown to non-dimensional values, they should apply reasonably well to other dimensional values of $l^{\mathrm{o}}_{\mathrm{h}}$ with the above caveats in mind.

2.3.3. *Application to the simple transport history*

Fig. 7A shows the results of applying the sampling function to our simple model mantle 10 000 times at sampling length scales of 10 and 100 km.

We first note that much of the higher-order structure has been filtered out in these plots. This results from the fact that the older subreservoirs, making up the outer part of the curves in Fig. 5, are less massive than the younger subreservoirs as a consequence of Eq. 23, and also from their short length scales, which limit their ability to dominate a large sample. We are left with a roughly linear anti-correlation between $\varepsilon_{\mathrm{Nd}}$ and $\varepsilon_{\mathrm{Sr}}$, the so-called 'mantle array'. We discuss this in more detail in Section 4.1.

In addition to observing the trend of the data in Nd–Sr space, it is useful to look at the distribution in one dimension in the form of a histogram. Fig. 7B shows histograms of measurements of $\varepsilon_{\mathrm{Nd}}$ for a system with $F=0.01$, sampled on various length scales. For short length scales, the distribution is bimodal, with the dominant peak plotting toward the depleted (high $\varepsilon_{\mathrm{Nd}}$) end of the graph. As the sampling length scale increases, however, the magnitude of this initially dominant peak de-

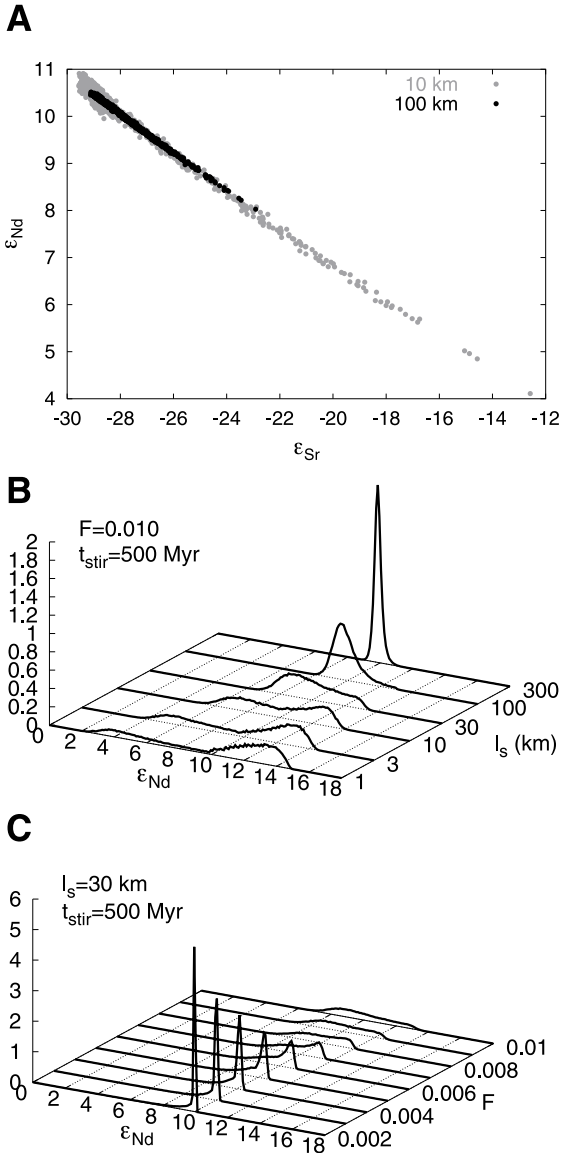

Fig. 7. (A) Synthetic geochemical data. Each point is the result of applying the sampling algorithm described in the text. We have assumed a linear evolution of the continental crust with no recycling. The melt fraction F is 0.005, and the sampling length scale is 10 or 100 km, as marked. (B) Histograms of synthetic data, binned at 0.1 ε units, for various values of l_{s}, with $F=0.01$. In these and all subsequent histograms, the vertical scale has been normalized such that the area under the curve is equal to one, effectively making the curves probability density functions. (C) Same as B, but l_{s} is a constant 30 km, and F is varied.

creases and the two modes merge into a single intermediate peak. Note that the changing shape of the distribution makes a characterization of the data in terms of mean and standard deviation difficult and somewhat misleading.

This behavior can be understood quite simply. The samples represent a mix between depleted subreservoirs and primitive material. The subreservoirs represent a very large volumetric fraction of the depleted mantle, but the chemical concentrations within them are very low. Conversely, the primitive mantle is volumetrically small, but the chemical concentrations therein are relatively high. When we sample on a short length scale, the observations frequently represent the sampling of a single depleted subreservoir, leading to the high values of the probability density function at the depleted end of the distribution. As the sampling length scale increases, it becomes increasingly difficult for the depleted subreservoirs to dominate any given sample. The samples tend to include mixtures of a larger number of subreservoirs along with primitive material. The relatively high chemical concentrations in the primitive mantle allow it to contribute in greater proportion than its relative mass, shifting the mean of the distribution to lower ε_{Nd} values. At $l_s = 300$ km, the distribution is very nearly Gaussian with the mode centered at $\varepsilon_{Nd} = 9.8$.

In Fig. 7C we investigate the dependence of the distribution on the melt fraction F. Assuming a constant sampling length scale l_s of 30 km, we vary F and again plot the histograms of the sample ε_{Nd} values. With greater melt fraction F, we observe a greater variability. In particular, the distribution stretches further towards depleted ε_{Nd} values. This can be understood in terms of two effects. First, as shown in Fig. 5B, the older subreservoirs have increasingly high ε_{Nd} values with greater melt fraction. Second, the masses of the older subreservoirs will be increasingly large with greater melt fraction. This effect is a direct result of Eq. 23: a higher melt fraction leads to a more rapid reduction in the mass of the existing subreservoirs, as well as the remaining mass of primitive material. Therefore, for small values of F, a large percentage of the mass of the depleted mantle is concentrated in the youngest subreservoirs, those whose ε_{Nd} and ε_{Sr} values are closest to the reservoir mean.

3. Application to a time-dependent transport history with recycling

In the previous section, we applied our model for the evolution of isotopic heterogeneity in the depleted mantle to a very simple transport history, that of uniform extraction of the continental crust. As this history was unidirectional, the only source of heterogeneity in the mantle was the residue from partial melting. We now examine the effects of continental crustal recycling, applying our method to the transport history presented in [11]. The transport history and the evolution of the mean continental crust and depleted mantle reservoirs are shown in Fig. 8.

3.1. Composition of the subreservoirs

Fig. 9A shows the full range of heterogeneity expected at various points in time, as in Fig. 5A. Because this transport history includes recycled

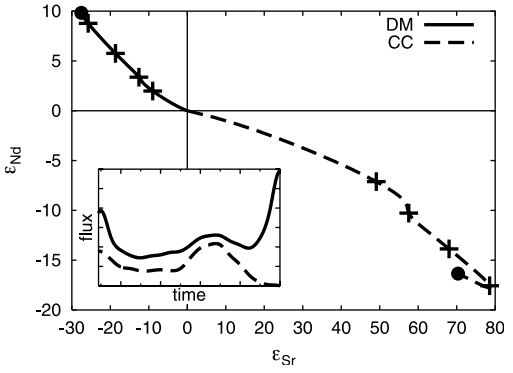

Fig. 8. Evolution of ε_{Nd} and ε_{Sr} in the mean depleted mantle (DM) and continental crust (CC), assuming the time-dependent history of bidirectional mass transport presented in [11] (compare with Fig. 3). The inset figure shows the transport history: the solid curve shows the rate of mass transport from the depleted mantle to the continental crust, while the dashed line shows the rate of crustal recycling. Time runs right to left, so the present day appears on the left end of the inset graph. The fluxes are scaled such that the integrated difference between the two curves is the present mass of the continental crust.

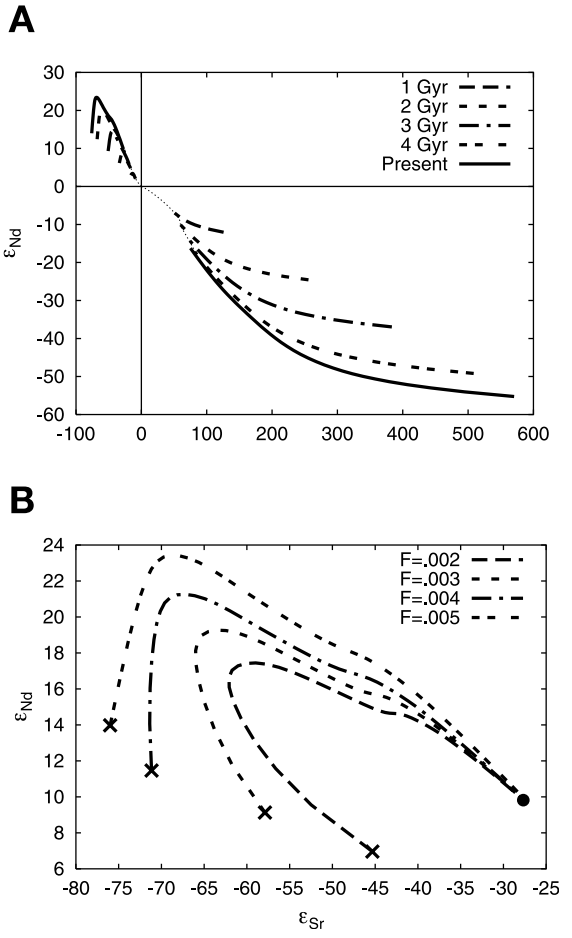

Fig. 9. The spectrum of heterogeneity generated in the depleted mantle by time-dependent crustal extraction with recycling of continental crust (compare with Fig. 5). (A) Heterogeneity at various times, assuming a melt fraction F of 0.005. Note that in this case there are subreservoirs with enriched isotopic compositions, due to the recycled material. (B) The effect of changing F on the isotopic composition of the depleted subreservoirs, for values of F ranging from 0.002 to 0.005 (see text for explanation). Because the composition of the enriched subreservoirs is dependent only on the continental evolution curve, which is independent of the melt fraction F, the present-day composition of the enriched subreservoirs will always fall on the solid curve in the lower right quadrant of A.

continental crust, we have subreservoirs that plot in the enriched (lower right) as well as the depleted (upper left) quadrant. We can expect much higher variance in this case, due both to these enriched components and the more highly depleted residual subreservoirs.

Again, we show the effects of changing F on the predicted heterogeneity. However, we only show isotopic values of the depleted subreservoirs; because the composition of the enriched subreservoirs is dependent only on the composition of the continental crust at the time of their creation, and this evolution is independent of F, the enriched subreservoirs will always fall on the solid curve in the lower right quadrant of Fig. 9A. Note that we have not shown any results for $F > 0.005$. Table 1 indicates that $d_{Rb23} = 200.0$ for this transport history. Such an enrichment is impossible if $F > 0.005$; even if all of the Rb in the source goes into the melt, the source region must be 200× larger than the melt to provide enough atoms. Thus, to the extent that this mass transport history is correct, it provides constraints on the process of continental crustal formation: however complicated this process, it must have the net effect of depleting a residue at least 200× greater than the continental crust created.

3.2. The sampled mantle

We show the results of sampling the model system in Fig. 10. When compared with the linear growth case (Fig. 7), these results show a greater spread in both the depleted and enriched quadrants. The difference between sampling on a 10 km and a 100 km scale is even more pronounced than it was previously. However, the linear anticorrelation between ε_{Nd} and ε_{Sr} remains. This strong linearity is a bit surprising, given the extreme non-linearity of Fig. 9, but again the oldest components are not volumetrically very significant and have the smallest associated length scales. These effects limit their ability to affect the isotopic composition of the samples.

We illustrate the sampling length scale dependence of the distribution in Fig. 10B. At shorter sampling lengths, the distribution is very skewed to the right, as the abundant depleted subreservoirs dominate the samples. As the length scale of sampling increases, the less abundant but more isotopically enriched low-ε_{Nd} subreservoirs have a greater effect. At $l_s = 100$ km, the distribution

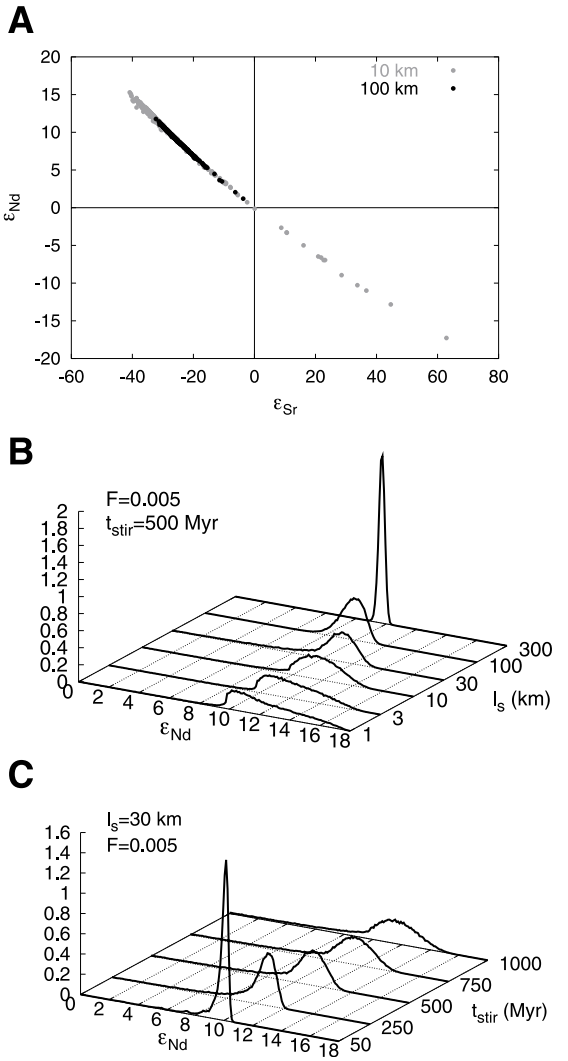

Fig. 10. (A) Synthetic geochemical data for a time-dependent evolution of the continental crust. Each point is the result of applying the sampling algorithm described in the text. The melt fraction F is 0.005, and the sampling length scale is 10 or 100 km, as marked. (B) Histograms of synthetic data sampled at various length scales. F is held constant at 0.005. (C) Histograms of synthetic data for various characteristic stirring times, given a melt fraction F of 0.005 and a sampling length scale l_s of 30. (Note that this is different from Fig. 7C, in which we vary F.) Shorter characteristic stirring times both tighten the distribution and shift the mode toward a more primitive composition.

is actually slightly skewed left. Finally, at $l_s = 300$ km, we recover the tight normal distribution observed earlier.

With this transport history, the effects of changing the effective melt fraction F are significantly muted. Increasing F increases the observed heterogeneity, but only slightly. We do not show these results here.

3.3. Sensitivity to stirring time

A significant amount of computational effort has been directed toward constraining rates of stirring in the mantle. These rates are meaningful, however, only insofar as they are reflected in geochemical observations.

Fig. 10C shows histograms reflecting the distribution of expected observations for various characteristic stirring times, given a melt fraction F of 0.005 and a sampling length scale l_s of 30 km. The samples, obtained by simulating 4.6 Gyr of mantle evolution with 10 Myr time steps, followed by taking 50 000 random samples of the depleted mantle so generated, are stacked in bins 0.1 ε units wide.

As expected, shorter stirring times lead to smaller variations in ε_{Nd}. In quantitative terms, a change in τ_{stir} from 1 Byr to 50 Myr reduces the standard deviation in observed ε_{Nd} values by about a factor of two. This change also shifts the mode of the distribution by close to two ε_{Nd} units. The volume of each of the subreservoirs remains the same in all the calculations; only the $l_{h2.i}$ change. Recall that the volume of each sub-subreservoir is $l^3_{h2.i}$. Therefore, the smaller values of $l_{h2.i}$ associated with shorter characteristic stirring times limit the ability of a single sub-subreservoir to dominate a given sample. Depleted subreservoirs, with their large initial length scales and low chemical concentrations, are particularly susceptible to this effect, giving rise to the asymmetry observed in Fig. 10C.

3.4. Quantitative inferences

If we assume that this flux history is correct, we can draw some inferences about the appropriate parameter values for the real Earth. Comparing

Fig. 10B with the mid-ocean ridge basalt (MORB) curve of Fig. 1, we conclude that values of l_s less than $\sim$30 km yield distributions whose skewness is inconsistent with the data. Sampling lengths l_s significantly greater than 100 km yield much tighter histograms than observed. Therefore, we feel reasonably confident putting bounds on the sampling length scale: 20 km $< l_s <$ 200 km. In non-dimensional terms, this corresponds to $1/5 < l_s/l^o_{h23} < 2$.

Comparing Fig. 10A with the MORB curve of Fig. 1, we can also put bounds on the stirring time, although there is some degree of trade-off between this parameter and the length scales mentioned above. It appears that 250 Myr and 750 Myr effectively bracket the range of values of τ_{stir} that reproduce something resembling the MORB curve. This range is in agreement with those found in numerical studies of mixing [41].

4. Discussion and conclusions

4.1. The mantle array revisited

The strong anti-correlation between ε_{Nd} and ε_{Sr} has been noted for some time [5–7] and dubbed the 'mantle array'. The two most popular explanations for this relationship are that it (a) results from a continuous differentiation process in which each component of the mantle lies on the mantle array and (b) represents a mixing line between two end-member compositions of nearly homogeneous composition [42–44]. Each of these applies strict conditions on the melting process to explain the observations.

In our model, none of these conditions holds in the strict sense, and yet we are able to recover an approximately linear trend. Despite the very non-linear appearance of a plot of the ε_{Nd} vs. ε_{Sr} values of the subreservoirs (e.g. Figs. 5 and 9), the sampling process eliminates most of this complexity, leaving behind the simple trend. This trend is a fairly robust feature (see below for exceptions) which therefore cannot be used to place strong restrictions on the melting process. We suggest a very inhomogeneous source region for the oceanic basalts, similar to the marble cake mantle of [37], with widely varying isotopic compositions and elemental concentrations that reduce to the simple linear trend in Nd–Sr space when sampled on a large enough length scale.

4.2. The ocean island basalts

Fig. 1B shows that there is a fundamental difference between the ocean island basalts (OIBs) and the mid-ocean ridge basalts (MORBs). The OIBs are less depleted on average than the MORBs, with a significant fraction actually showing enriched compositions. In addition, the OIBs appear to be more heterogeneous than the MORBs, with a broader, less peaked histogram.

One should exercise caution in interpreting the OIB data, as they are not randomly distributed geographically. As a more thorough evaluation of the data is beyond the scope of this work, however, we will take the data at face value and assume that they are representative of the OIB source region.

One possible explanation of the greater isotopic heterogeneity exhibited by the OIBs is that the sampling length scale of OIBs could be shorter than that of MORBs. Fig. 10 shows that shorter sampling lengths correspond to a broader distribution of isotopic measurements. However, these broader distributions are always accompanied by a shift of the mean toward more depleted compositions. This is exactly the opposite of what is observed in the OIBs, whose composition is less depleted than the MORBs. Therefore, we can reject this hypothesis.

There are two non-mutually exclusive explanations for the less depleted character of the OIBs. The first is a simple difference in melting process. If OIBs represent a smaller melt fraction of the source region than the MORBs, they may tap the more enriched components contained therein. The second is that the OIBs tap an additional, less depleted source region. In our models, this region would correspond to the roughly 2/3 of the mantle that does not participate in the creation of continental crust.

Focusing on the second explanation, we can model the OIBs as a mixture between the undepleted mantle and our depleted, heterogeneous

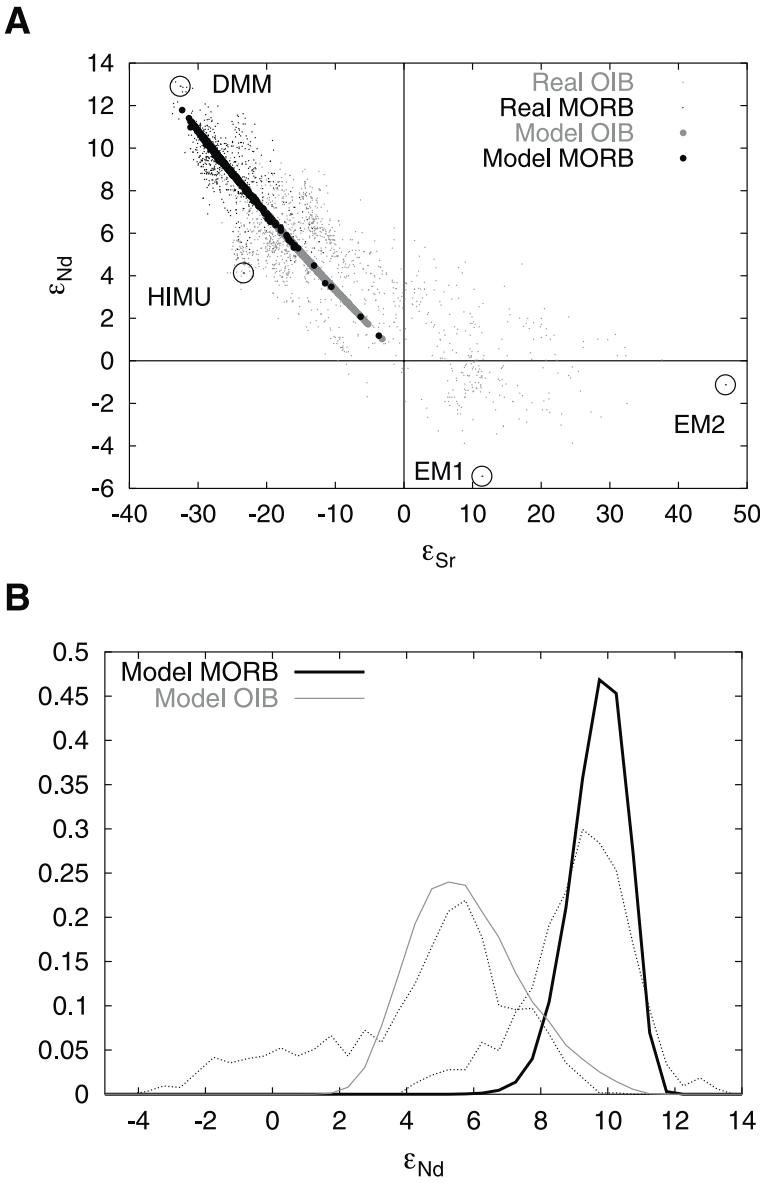

Fig. 11. (A) Model MORB and OIB data plotted on real data. By increasing the source region available to the OIBs, we shift the distribution towards the undepleted composition. These calculations employ the time-dependent mass transport history with continental recycling and assume a 100 km sampling length scale. (B) Histograms of the model data shown above. The light, dotted curves represent the real histograms, as previously shown in Fig. 1A. In both cases we fail to reproduce some of the less depleted or more enriched material observed in the real data.

MORB source region. One simple way to go about this is to assume that the OIBs simply have access to a greater fraction of the mantle. We apply the same sampling function as before, but we increase the total volume of the source region by 45% (chosen so that the peak of the distribution would match observations) and assume that any new material in the source region is undepleted. The results of this experiment are shown in Fig. 11.

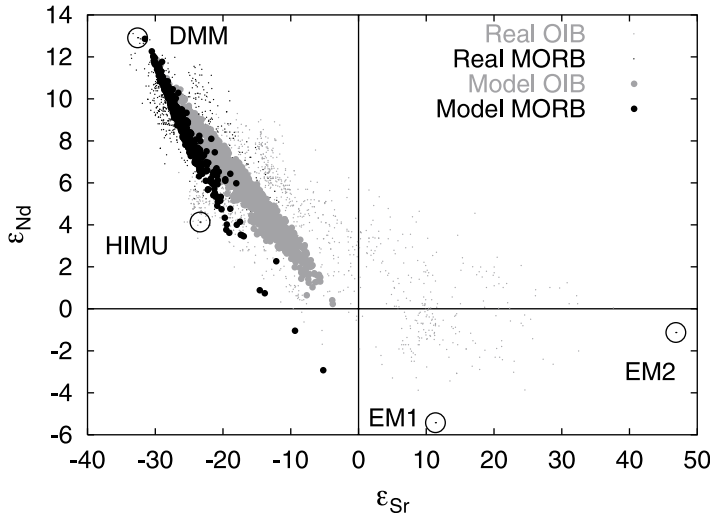

Fig. 12. Synthetic data from our preferred model. All parameters identical to those in Fig. 11 but recycled continental crustal material is enriched in Sm, Nd, and Rb, and depleted in Sr relative to the bulk continental crust.

This model fits the data reasonably well. In the OIB case, however, the model fails to reproduce a significant number of more isotopically enriched observations. Choosing a shorter sampling length scale for the OIBs could alleviate this discrepancy somewhat, but would also increase the number of highly depleted samples, contrary to observation. We conclude instead that our model must be neglecting the process(es) that produced the more enriched OIBs.

Despite the fact that at least 1/3 of the OIB source region in this model consists of completely undepleted material, we never observe samples that are completely undepleted. The oldest subreservoirs are so well mixed that they contribute to any sample one takes. It has been argued that the absence of samples showing a completely primitive signature indicates that no primitive material remains in the mantle. Our results suggest that it may be possible for significant fractions of the sampled mantle to remain primitive and yet not be discernible as such at the surface.

4.3. A more heterogeneous model: recycled terrigenous sediments

While the previous models have been successful in reproducing the trend in the oceanic basalt data and the differences between MORBs and OIBs, the real data are not nearly so well behaved as our model system. There is a great deal of scatter about the main trend in the data. In addition, there appears to be some concavity in the data which is not as pronounced in our model.

We believe it is likely that the recycled continental crust is dominated by terrigenous sediment that is derived primarily from the upper crust and transported as suspended load in rivers to subduction zones, where it is injected into the mantle. Taylor and McLennan [45] and Rudnick and Fountain [46] show that the upper crust is enriched in Rb, Sm, and Nd relative to the bulk continental crust, whereas the concentration of Sr is relatively uniform throughout. In addition, Rb, Sm, and Nd have limited mobility in weathering, implying that they tend to remain in suspended sediments; Sr is highly mobile and rapidly lost to solution. These effects lead to a suspended load which is enriched in Rb, Sm, and Nd and depleted in Sr relative to the bulk continental crust, as observed by Goldstein and Jacobsen [47]. If this material dominates the recycled continental crust, the recycled component will correspondingly reflect these compositions.

We model this situation by changing the d_{i32} enrichment factors so that $d_{\mathrm{Sm32}} > 1$, $d_{\mathrm{Nd32}} > 1$,

$d_{Rb32} > 1$, and $d_{Sr32} < 1$ (all of these were equal to one in all previous calculations). Adjusting these values as listed in Table 1 leads to the model results shown in Fig. 12.

This model reproduces some of the concavity observed in the data by generating two distinct trends in the data: a MORB trend and an OIB trend. Linear regression on the MORB and OIB data indicates that the MORB array is indeed steeper in Sr–Nd space than the OIB array. However, it is unclear whether this difference represents two distinct linear arrays or merely different portions of a continuous curve.

One implication of this result is that it may be dangerous to use the mantle array to define the $^{87}Sr/^{86}Sr$ and Rb/Sr ratios of the bulk silicate Earth as was done by DePaolo and Wasserburg [5] and O'Nions et al. [7]. It is possible to have a linear trend in Nd–Sr space which does not point to the origin. Rather, it may represent the extreme end of a mixing curve which only appears locally linear.

This model also reproduces some of the scatter about the main trend, but it still fails to explain many of the more isotopically enriched observations, particularly those trending towards the proposed EM2 end member.

4.4. Limitations of the models presented

Because we introduce a new methodology in this paper, we have kept the models as simple as possible. We stress, however, that many of the limitations of the models shown can be easily removed in the future.

In modeling the generation of continental crust, we have chosen to fold all the complexity of what is likely a multi-stage and time-dependent phenomenon into a single parameter F. Our method is flexible enough, however, that the future inclusion of a more complicated melting model, if justified, would be straightforward.

Our sampling model neglects potential mineralogical effects. Depleted subreservoirs are likely to have a higher solidus than the enriched subreservoirs, making the latter likely to dominate a sample created by partial melting. It may be valid to incorporate a fertility function to parameterize these effects. However, the very low chemical concentrations in the depleted subreservoirs already limit their contribution to any mixture, so these effects are likely to be small.

These models have focused on the heterogeneity associated with the creation and recycling of continental crust. We have chosen to neglect the generation of oceanic crust and the heterogeneity associated therewith. This process is especially important in the U–Th–Pb system and will be investigated in future work.

All of the calculations shown in this paper assume that only 1/3 of the mantle has been depleted to create the continental crust. This is consistent with mass balance data, although current uncertainties allow the depleted portion of the mantle to be significantly larger. We reiterate that this assumption does not imply anything geometrically about the structure of the mantle; the 'blob' model of Becker et al. [48], the 'stagnant core' model of Spohn and Schubert [49], and a layered mantle all look the same in a reservoir formulation. Neither is this assumption central to our model here. One could just as well choose a hot abyssal layer [26] or the enriched D′ model of Coltice and Richard [50]. However, those models introduce new assumptions about the evolution of the enriched layer, complexities we elect to avoid at this stage.

Finally, we have limited ourselves to the well-behaved Sm–Nd and Rb–Sr systems. The simple flux models we have used will not be sufficient to explain even the bulk behavior of the U–Th–Pb system or the noble gases. The application of the methods presented here to those systems will be the topic of a later paper.

4.5. Summary

There are two complementary approaches to improving our understanding of the Earth through geochemistry: expanding the data set and improving our models. This paper seeks to expand our modeling capabilities so that we can take better advantage of the geochemical data already present. Specifically, it allows us to consider the distribution of isotopic measurements as a reflection of the processes at work.

This work builds on the conventional reservoir models of geochemistry, which track the evolution of the mean isotopic concentrations in various hypothetical Earth reservoirs. By applying basic understandings gained from dynamical studies of mixing in the Earth, we are able to quantify the processes that create and destroy chemical heterogeneity in the Earth's mantle. Ultimately, we are able to generate synthetic distributions of isotopic data which can be compared directly with real data.

Our models predict much of the observed complexity in the Rb–Sr and Sm–Nd systems, including some higher-order features. The mantle array and even the deviations from it fall quite naturally out of the simple cases considered here. We are able to place limits on the ratio of heterogeneity length scale to sampling length scale, as well as on the stirring time of the mantle. Sampling length scale alone is unable to explain the more enriched character of the OIBs with respect to MORBs. However, by increasing the size of the source region of the OIBs, we are able to reproduce the main offset.

Acknowledgements

This manuscript greatly benefitted from reviews by Donald DePaolo and Francis Albarède as well as the constructive comments of Gerald Wasserburg, Thorsten Becker, and Matthieu Dumberry. This work was supported by funding from NSF Cooperative Studies of the Earth's Deep Interior (EAR 0112563), NSF Geophysics (EAR 9814666), and the Institute of Geophysics and Planetary Physics at the Los Alamos National Laboratory.***[BOYLE]***

References

[1] F. Albarède, R.D. van der Hilst, New mantle convection model may reconcile conflicting evidence, EOS Trans. AGU 80 (1999) 535–539.
[2] P.J. Tackley, Mantle convection and plate tectonics: Towards an integrated physical and chemical theory, Science 288 (2000) 2002–2007.
[3] P.E. van Keken, E.H. Hauri, C.J. Ballentine, Mantle mixing: the generation, preservation, and destruction of chemical heterogeneity, Annu. Rev. Earth Planet. Sci. 30 (2002) 493–525.
[4] A. Zindler, S. Hart, Chemical geodynamics, Annu. Rev. Earth Planet. Sci. 14 (1986) 493–571.
[5] D.J. DePaolo, G.J. Wasserburg, Inferences about magma sources and mantle structure from variations of $^{143}Nd/^{144}Nd$, Geophys. Res. Lett. 3 (1976) 743–746.
[6] P. Richard, N. Shimizu, C.J. Allègre, $^{143}Nd/^{144}Nd$, a natural tracer: an application to oceanic basalts, Earth Planet. Sci. Lett. 31 (1976) 269–278.
[7] R.K. O'Nions, P.J. Hamilton, N.M. Evensen, Variations in $^{143}Nd/^{144}Nd$ and $^{87}Sr/^{86}Sr$, Earth Planet. Sci. Lett. 34 (1977) 13–22.
[8] S.B. Jacobsen, G.J. Wasserburg, The mean age of mantle and crustal reservoirs, J. Geophys. Res. 84 (1979) 7411–7427.
[9] R.K. O'Nions, N.M. Evensen, P.J. Hamilton, Geochemical modeling of mantle differentiation and crustal growth, J. Geophys. Res. 84 (1979) 6091–6101.
[10] D.J. DePaolo, Crust growth and mantle evolution: Inferences from models of element transport and Nd and Sr isotopes, Geochim. Cosmochim. Acta 44 (1980) 1185–1196.
[11] S.B. Jacobsen, Isotopic and chemical constraints on mantle-crust evolution, Geochim. Cosmochim. Acta 52 (1988) 1341–1350.
[12] S.B. Jacobsen, Isotopic constraints on crustal growth and recycling, Earth Planet. Sci. Lett. 90 (1988) 315–329.
[13] F. Albarède, Introduction to Geochemical Modeling, Cambridge University Press, Cambridge, 1995.
[14] F. Albarède, Time-dependent models of U-Th-He and K-Ar evolution and the layering of mantle convection, Chem. Geol. 145 (1998) 413–429.
[15] F. Albarède, Radiogenic ingrowth in systems with multiple reservoirs: applications to the differentiation of the mantle-crust system, Earth Planet. Sci. Lett. 189 (2001) 59–73.
[16] F.M. Richter, S.F. Daly, H.-C. Nataf, A parameterized model for the evolution of isotopic heterogeneities in a convecting system, Earth Planet. Sci. Lett. 60 (1982) 178–194.
[17] M. Gurnis, Mixing in numerical models of mantle convection incorporating plate kinematics, J. Geophys. Res. 91 (1986) 6375–6395.
[18] M. Gurnis, Stirring and mixing in the mantle by plate-scale flow: large persistent blobs and long tendrils coexist, Geophys. Res. Lett. 13 (1986) 1474–1477.
[19] D. McKenzie, Finite deformation during fluid flow, J.R. Astron. Soc. 58 (1979) 589–715.
[20] N.R.A. Hoffman, D.P. McKenzie, The destruction of geochemical heterogeneities by differential fluid motions during mantle convection, Geophys. J. R. Astron. Soc. 82 (1985) 163–206.
[21] L.H. Kellogg, D.L. Turcotte, Mixing and the distribution of heterogeneities in a chaotically convecting mantle, J. Geophys. Res. 95 (1990) 421–432.

[22] P.E. van Keken, C.J. Ballentine, Dynamical models of mantle volatile evolution and the role of phase transitions and temperature dependent rheology, J. Geophys. Res. 104 (1999) 7137–7168.
[23] S. Ferrachat, Y. Ricard, Mixing properties in the Earth's mantle: Effects of the viscosity stratification and of oceanic crust segregation, Geochem. Geophys. Geosyst. 2 (2001) 2000GC000092.
[24] U. Christensen, A.W. Hofmann, Segregation of subducted oceanic crust in the convective mantle, J. Geophys. Res. 99 (1994) 19867–19884.
[25] P.J. Tackley, Three-dimensional simulations of mantle convection with a thermochemical CMB boundary layer: D″?, in: M. Gurnis (Ed.), The Core-Mantle Boundary Region, American Geophysical Union, 1998, pp. 231–253.
[26] L.H. Kellogg, B.H. Hager, R.D. van der Hilst, Compositional stratification in the deep mantle, Science 283 (1999) 1881–1884.
[27] P.E. van Keken, S.D. King, H. Schmeling, U. Christensen, D. Neumeister, M.-P. Doin, A comparison of methods for the modeling of thermochemical convection, J. Geophys. Res. 102 (1997) 22477–22496.
[28] C.J. Allègre, E. Lewin, Istopic systems and stirring times of the Earth's mantle, Earth Planet. Sci. Lett. 136 (1995) 629–646.
[29] C.J. Allègre, M. Moreira, T. Staudacher, 4He/3He dispersion and mantle convection, Geophys. Res. Lett. 22 (1995) 2325–2328.
[30] P. Olson, D.A. Yuen, D. Balsinger, Mixing of passive heterogeneities by mantle convection, J. Geophys. Res. 89 (1984) 425–436.
[31] A.W. Hofmann, Mantle geochemistry the message from oceanic volcanism, Nature 385 (1997) 219–229.
[32] W.H. Press, S.A. Teukolsky, W.T. Vetterling, B.P. Flannery, Numerical Recipes in Fortran: The Art of Scientific Computing, Cambridge University Press, 1992.
[33] R.L. Rudnick, Making continental crust, Nature 378 (1995) 571–578.
[34] A.W. Hofmann, S.R. Hart, An assessment of local and regional isotopic equilibrium in the mantle, Earth Planet. Sci. Lett. 38 (1978) 44–62.
[35] L.H. Kellogg, D.L. Turcotte, Homogenization of the mantle by convective mixing and diffusion, Earth Planet. Sci. Lett. 81 (1986/1987) 371–378.
[36] P.E. van Keken, S. Zhong, Mixing in a 3[d] spherical model of present-day mantle convection, Earth Planet. Sci. Lett. 171 (1999) 533–547.
[37] C.J. Allègre, D.L. Turcotte, Implications of a two-component marble-cake mantle, Nature 323 (1986) 123–127.
[38] U. Christensen, Mixing by time-dependent convection, Earth Planet. Sci. Lett. 95 (1989) 382–394.
[39] C.W. Gable, H.A. Stone, R.J. O'Connell, Chaotic mantle mixing; time dependence is unnecessary, EOS Trans. AGU 72 (1991) 296.
[40] S. Ferrachat, Y. Ricard, Regular vs. chaotic mantle mixing, Earth Planet. Sci. Lett. 155 (1998) 75–86.
[41] J.B. Kellogg, R.J. O'Connell, The effects of toroidal motion and layered viscosity on mixing in three dimensions, EOS Trans. AGU 80 (2000) Abstract T21A-09.
[42] D.J. DePaolo, Implications of correlated Nd and Sr isotopic variations for the chemical evolution of the crust and mantle, Earth Planet. Sci. Lett. 43 (1979) 201–211.
[43] S.B. Jacobsen, G.J. Wasserburg, Nd and Sr isotopic study of the Bay of Islands ophiolite complex and the evolution of the source of midocean ridge basalts, J. Geophys. Res. 84 (1979) 7429–7445.
[44] C.J. Allègre, O. Brévart, B. Dupré, J.-F. Minster, Isotopic and chemical effects produced in a continuously differentiating convecting Earth mantle, Philos. Trans. R. Soc. Lond. A 297 (1980) 447–477.
[45] S.R. Taylor, S.M. McLennan, The geochemical evolution of the continental crust, Rev. Geophys. 33 (1995) 241–265.
[46] R.L. Rudnick, D.M. Fountain, Nature and composition of the continental crust - a lower crustal perspective, Rev. Geophys. 33 (1995) 267–309.
[47] S.J. Goldstein, S.B. Jacobsen, Nd and Sr isotopic systematics of river water suspended material: implications for crustal evolution, Earth Planet. Sci. Lett. 87 (1988) 249–265.
[48] T.W. Becker, J.B. Kellogg, R.J. O'Connell, Thermal constraints on the survival of primitive blobs in the lower mantle, Earth Planet. Sci. Lett. 171 (1999) 351–365.
[49] T. Spohn, G. Schubert, Modes of mantle convection and the removal of heat from the Earth's interior, J. Geophys. Res. 87 (1982) 4682–4696.
[50] N. Coltice, Y. Ricard, Geochemical observations and one layer mantle convection, Earth Planet. Sci. Lett. 174 (1999) 125–137.